Summer surface air temperature proxies point to near sea-ice-free conditions in the Arctic at 127 ka.

Louise C. Sime[1], Rahul Sivankutty[1], Irene Vallet-Malmierca[1], Agatha M. de Boer[2], and Marie Sicard[2]

[1]British Antarctic Survey, Cambridge, UK

[2]Department of Geological Sciences, Stockholm University, Sweden.

Correspondence: Louise C. Sime (lsim@bas.ac.uk)

Abstract.

11 The Last Interglacial (LIG) period, which had higher summer solar insolation than today, has been

12 suggested as the last time that Arctic summers were ice-free. However, the latest suite of Coupled

13 Modelling Intercomparison Project 6 Paleoclimate (CMIP6-PMIP4) simulations of the LIG produce a

14 wide range of Arctic summer minimum sea ice area (SIA) results, ranging from a 30% to 96%

15 reduction from the pre-industrial (PI). Sea ice proxies are also currently neither abundant nor

16 consistent enough to determine the most realistic state. Here we estimate LIG minimum SIA

17 indirectly through the use of 21 proxy records for LIG Summer Surface Air Temperature (SSAT) and

18 11 CMIP6-PMIP4 models for the LIG. We use two approaches. First, we use two tests to determine

19 how skilful models are at simulating reconstructed ΔSSAT from proxy records (where Δ refers to

20 LIG-PI). This identifies a positive correlation between model skill and the magnitude of ΔSIA: the

21 most reliable models simulate a larger sea ice reduction. Averaging the most skilful two models yields

22 an average SIA of 1.3 mill. km^2 for the LIG. This equates to a 4.5 mill. km^2, or a 79%, SIA reduction

23 from the PI to the LIG. Second, across the 11 models, the averaged ΔSSAT at the 21 proxy locations

24 as well the pan Arctic average ΔSSAT, is inversely correlated with ΔSIA (r = -0.86 and -0.79

25 respectively). In other words, the models show that a larger Arctic warming is associated with a

26 greater sea ice reduction. Using the proxy record-averaged ΔSSAT of 4.5 $\pm$ 1.7 K and the relationship

27 between ΔSSAT and ΔSIA suggests an estimated sea ice reduction of 4.2$\pm$1.4 mill. km^2 or about 74%

28 less sea ice than the PI. The mean proxy-location ΔSSAT is well-correlated with the Arctic-wide

29 ΔSSAT north of 60°N (r=0.97) and this relationship is used to show that the mean proxy record

30 ΔSSAT is equivalent to an Arctic-wide warming of 3.7$\pm$1.5 K at the LIG compared to the PI.

31 Applying this Arctic-wide ΔSSAT and its modelled relationship to ΔSIA, results in a similar estimate

32 of LIG sea ice reduction of 4.1$\pm$1.2 mill. Km^2. These LIG climatological minimum SIA of 1.3 to 1.5

33 mill. km^2 are close to the definition of a summer ice-free Arctic, which is a maximum sea ice extent

34 less than 1 mill. km^2. The results of this study thus suggest that the Arctic likely experienced a

35 mixture of ice-free and near ice-free summers during the LIG.

1. Introduction

The rapid decline in Arctic sea ice over the last 40 years is an icon of contemporary climate change. Climate models have struggled to fully capture this sea ice loss (Notz and Community, 2020), which can sometimes reduce confidence in their future projections (*e.g.* IPCC, 2021). One line of investigation to address this problem, that has not been fully exploited, is the use of past climates to provide information on the future (e.g. Bracegirdle et al., 2019). Investigating the physics and causes of sea ice change, concentrating on Arctic changes during the most recent warm climate periods can help us address this problem (Guarino et al., 2020b). Interglacials are periods of globally higher temperatures which occur between cold glacial periods (Sime et al., 2009; Otto-Bliesner et al., 2013; Fischer et al., 2018). The differences between colder glacial and warmer interglacial periods are driven by climate feedbacks alongside changes in the Earth's orbit which affect incoming radiation. The Last Interglacial or LIG, occurred 130,000-116,000 years ago. At 127,000 years ago, at high latitudes orbital forcing led to summertime top-of-atmosphere shortwave radiation 60–75 Wm^{-2} greater than the PI period. Summer temperatures in the Arctic during the LIG are estimated to be around 4.5 K above those of today (CAPE members, 2006; Kaspar et al., 2005; IPCC, 2013; Capron et al., 2017). Prior to 2020, most climate models simulated summer LIG temperatures which were too cool compared with these LIG temperature observations (Otto-Bliesner et al., 2013; IPCC, 2013). This led Lunt et al. (2013); Otto-Bliesner et al. (2013) and IPCC (2013) to suggest that the representation of dynamic vegetation changes in the Arctic might be key to understanding LIG summertime Arctic warmth.

Guarino et al. (2020b) argued that loss of Arctic sea-ice in the summer could cause the warm summer Arctic temperatures, without the need for dynamic vegetation. Using the HadGEM3 model, which was the UK's contribution for the LIG CMIP6-PMIP4 project, Guarino et al. (2020b) found that the model simulated a fully sea ice-free Arctic during the summer, i.e. it had less than 1 mill. km^2 of sea ice extent at its minimum. This unique, near complete, loss of summer sea ice appears to happen in the UK model, because it includes a highly advanced representation of melt ponds (Guarino et al. 2020b; Diamond et al. 2021). These are shallow pools of water which form on the surface of Arctic

65 sea ice and which determine how much sunlight is absorbed or reflected by the ice (Guarino et al.,
66 2020b).

67

68 Malmierca-Vallet et al. (2018) found the signature of summertime Arctic sea ice loss in Greenland ice
69 cores. Kageyama et al. (2021) then led the international community in compiling all available marine
70 core Arctic sea ice proxy data for the LIG and testing it against CMIP6-PMIP4 simulations. The
71 Kageyama et al. (2021) synthesis of ocean core-based proxy records of LIG Arctic sea-ice change,
72 like Malmierca-Vallet et al. (2018), showed that compared to the PI it is very likely that Arctic sea ice
73 was reduced. However, Kageyama et al. (2021) also showed that directly determining sea-ice changes
74 from marine core data is difficult. The marine core observations suffer some conflicting
75 interpretations of proxy data sometimes from the same core, and imprecision in dating materials to the
76 LIG period in the high Arctic. Thus, determining the mechanisms and distribution of sea ice loss
77 during the LIG by directly inferring sea ice presence (or absence) from these preserved biological data
78 alone is not possible (Kageyama et al., 2021).

79

80 The Coupled Model Intercomparison Project Phase 6 (CMIP6) Paleoclimate Model Intercomparison
81 Project Phase (PMIP4) or CMIP6-PMIP4 LIG experimental protocol prescribes differences between
82 the LIG and PI in orbital parameters, as well as differences in trace greenhouse gas concentrations
83 (Otto-Bliesner et al., 2017). This standardised climate modelling protocol is therefore an ideal
84 opportunity for the community to use models to explore the causes of Arctic warmth using multi-
85 model approaches. In particular, the existing non-dynamic-vegetation PMIP4 LIG protocol and
86 associated simulations offer the opportunity to address the question of whether the Arctic sea ice loss
87 alone is sufficient to explain LIG summertime temperature observations, or whether active vegetation
88 modelling, and the idea of vegetation feedbacks (Lunt et al., 2013; Otto-Bliesner et al.,2013; IPCC,
89 2013) are required. This said, we recognize that in reality there must also be LIG Arctic vegetation
90 feedbacks. These should be explored in future modelling work.

91

92   Guarino et al. (2020b) showed that the HadGEM3, the only CMIP-PMIP4 model with an ice-free
93   Arctic at the LIG, has an excellent match with reconstructed Arctic air temperature in summer. The
94   average ΔSSAT in HadGEM3, for all locations with proxy observations, is +4.9 ± 1.2 K compared
95   with the proxy mean of +4.5 ± 1.7 K. This model also matched all, except one, marine core sea-ice
96   datapoints from Kageyama et al. (2021). Here we investigate whether there are more CMIP6-PMIP4
97   models with a similarly good ΔSSAT and if so, whether other models with a good match also suggest
98   a much-reduced sea ice area (SIA) during the LIG. We further compute the correlation and linear
99   relationship in the models between ΔSSAT and ΔSIA and subsequently use this equation and proxies
100   for ΔSSAT to estimate ΔSIA. Section 2 describes the proxy data and models used in this study as well
101   as the analysis methods. The results are presented in Section 3 which first evaluates the modelled PI
102   and LIG sea ice distribution against proxy reconstructions and then use the above described
103   approaches to estimate the sea ice reduction at the LIG. Section 4 summarises the results and
104   discusses their shortcomings and implications.
105

106   **2. Data and methods**

107   **2.1 Proxy reconstructions for LIG**

108   The LIG SSAT proxy observations used to assess LIG Arctic sea ice in the Guarino et al. (2020b)
109   study were previously published by CAPE members (2006); Kaspar et al. (2005) and 20 of them were
110   also used to assess CMIP5 models in the IPCC (2013) report. A detailed description of each record is
111   available (CAPE members, 2006; Kaspar et al., 2005; IPCC, 2013; Capron et al., 2017). Each proxy
112   record is thought to be of summer LIG air temperature anomaly relative to present day and is located
113   in the circum-Arctic region; all sites are from north of 51°N. There are 7 terrestrial based temperature
114   records; 8 lacustrine records; 2 marine pollen-based records; and 3 ice core records included in the
115   original IPCC (2013) compilation. Guarino et al. (2020b) added to this an additional new record from
116   the NEEM Greenland ice core from Capron et al. (2017), bringing the total number of proxies records
117   to 21 (Table 1). Figure 1 shows the location, and type, for each numbered proxy record. Terrestrial
118   climate can be reconstructed from diagnostic assemblages of biotic proxies preserved in lacustrine,

119   peat, alluvial, and marine archives and isotopic changes preserved in ice cores and marine and

120   lacustrine carbonates (CAPE, 2006; Guarino et al., 2020). Quantitative reconstructions of climatic

121   departures from the present-day are derived from range extensions of individual taxa, mutual climatic

122   range estimations based on groups of taxa, and analogue techniques (CAPE, 2006). These proxy

123   records are considered to represent the summer surface air temperature because summer temperature

124   is also the most effective predictor for most biological processes, though seasonality and moisture

125   availability may influence phenomena such as evergreen vs. deciduous biotic dominance (Kaplan et

126   al., 2003). Whilst the exact timing of this peak warmth has not yet been definitively determined, it is

127   reasonable to assume that these measurements are approximately synchronous across the Arctic. It is

128   however very unlikely that the peak warmth was synchronous across both hemispheres (see Capron et

129   al. (2014); Govin et al. (2015)), and further investigation of the synchronicity of peak warmth occurs

130   across the Northern Hemisphere is merited. For consistency with modelled data, temperature

131   anomalies computed against present day conditions (i.e. 1961-1990 baseline) were corrected to

132   account for a +0.4K of global warming between PI (1850) and present day (1961-1990).(Turney and

133   Jones, 2010). Therefore, Table 1 and Guarino et al. (2020b) values differ slightly (+0.4K) from the

134   original datasets so that they represent temperature anomalies relative to the PI.

135

136
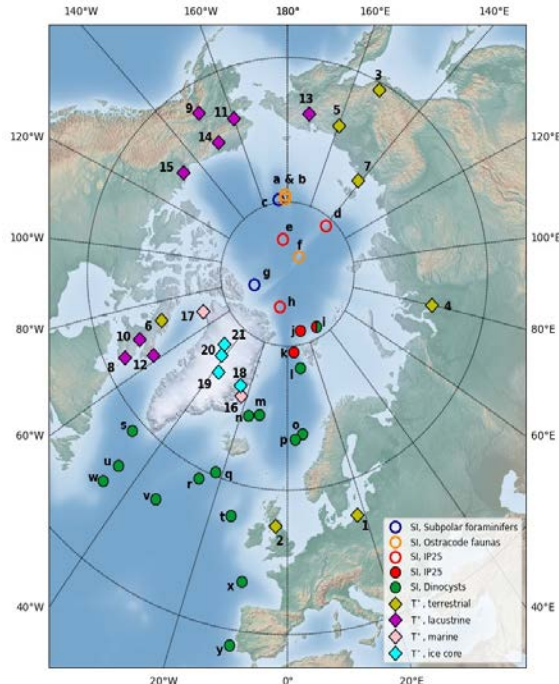
Figure 1: Map of data locations numbered to match Table 1. This combines the Kageyama et al. (2021) sea ice locations 1 to 20 alongside with the temperature proxies from Table 1. Open symbols correspond to records with uncertain chronology, and filled symbols correspond to records with good chronology.

Most of the sites have temperature uncertainty (one standard deviation) estimates, which are provided in the Table 1. However, for 9 sites, the standard deviation of the temperature data was not available. A standard deviation of ± 0.5K was used to account for this missing uncertainty: this is the smallest standard deviation found in any proxy record across all sites, and is thus as a conservative estimation of the uncertainty associated to proxy data (Guarino et al., 2020b).

146

147 *Table 1: Compilation of LIG-PI summertime surface air temperature (SSAT) anomalies used by*

148 *Guarino et al. (2020b).*

Number	Lat	Lon	Site	Observation type	Observation (K)
1	55	18	Europe	Terrestrial: pollen, plant macrofossils	3.4 ± 0.5
2	55	-3	UK	Terrestrial: Pollen, plant macrofossils	2.4 ± 0.5
3	61	152.5	Magadan	Terrestrial: pollen	6.4 ± 2
4	68	80	West-central Siberia	Terrestrial: pollen, plant macrofossils	5.4 ± 2
5	68	160	Northeast Siberia	Terrestrial: pollen	6.4 ± 2
6	70	-72.5	Flitaway	Terrestrial: insects, plant remains	4.9 ± 0.5
7	73.33	141.5	Bolshoy Lyadhovshy	Terrestrial: pollen	4.9 ± 0.5
8	63	-66	Robinson Lake	Lacustrine: pollen	5.4 ± 0.5
9	64	-150	Birch Creek/ky11	Lacustrine: pollen	1.4 ± 1
10	66	-69.2	Amarok Lake	Lacustrine: pollen	4.9 ± 0.5
11	67	-160	Squirrel Lake	Lacustrine: pollen, plant macrofossils	1.9 ± 1.5
12	67	-62	Cumber	Lacustrine: pollen	5.9 ± 1.5
13	67.5	172.08	Lake Elgygytgyn	Lacustrine: pollen	3.4 ± 1
14	69	-151	Ahaliorak Lake	Lacustrine: pollen	1.9 ± 1.5
15	69	-133	Lake Tuk 5	Lacustrine: plant macrofossils and beetles	2.4 ± 0.5
16	71.75	-23	Jameson	Marine: pollen, plant macrofossils, beetles, other invertebrates	5.4 ± 0.5
17	76.35	-68.3	Thule	Marine: pollen, chironomids	4.4 ± 0.5
18	73	-25	Renland	Ice core: d18O, dD	5.4 ± 0.5
19	73	-38	GISP2	Ice core: d18O, dD	5.4 ± 0.5
20	75	-42	NGRIP	Ice core: d18O, dD	5.4 ± 0.5
21	76.4	-44.8	NEEM(ds)	Ice core: d18O, dD	8 ± 4
-	-	-	Arctic	Mean of observations 1 to 21	4.5 ± 1.7

149

150

2.2. Models and model output

152 We analyse Tier 1 LIG simulations, based on the standard CMIP6-PMIP4 LIG experimental protocol

153 (Otto-Bliesner et al., 2017). The prescribed LIG (127 ka) protocol differs from the CMIP6 PI

154 simulation protocol in astronomical parameters and the atmospheric trace GHG concentrations. LIG

155 astronomical parameters are prescribed according to orbital constants (Berger and Loutre, 1991), and

156 atmospheric trace GHG concentrations are based on ice core measurements: 275 ppm for CO_2; 685

157 ppb for CH_4; and 255 ppb for N_2O (Otto-Bliesner et al., 2017).

158

159 The CMIP6-PMIP4 model simulations were run following the Otto-Bliesner et al. (2017) protocol,

160 except CNRM-CM6-1, which used GHG at their PI values rather than using LIG values. For all

161 models, all other boundary conditions, including solar activity, ice sheets, aerosol emissions etc., are

162 identical to the PI simulation. In terms of the Greenland and Antarctica ice sheets, a PI configuration

163 for the LIG simulation is not unreasonable (Kageyama et al., 2021; Otto-Bliesner et al., 2020). LIG

164 simulations were initialized either from a previous LIG run, or from the standard CMIP6 protocol PI

165 simulations, using constant 1850 GHGs, ozone, solar, tropospheric aerosol, stratospheric volcanic

166 aerosol and land use forcing. Whilst PI and LIG spin-ups vary between the models, with CNRM the

167 shortest at 100 years, most model groups aimed to allow the land and oceanic masses to attain

168 approximate steady state *i.e.* to reach atmospheric equilibrium and to achieve an upper-oceanic

169 equilibrium - which generally seems to take around 300 to 400 years. LIG production runs are all

170 between 100-200 years long, which is an appropriate length for Arctic sea ice analysis (Guarino et al.,

171 2020a).

172

173 Whilst fifteen models have run the CMIP6-PMIP4 LIG simulation (Kageyama et al., 2021; Otto-

174 Bliesner et al., 2020), and have uploaded model data to the Earth System Grid Federation (ESGF), we

175 exclude four simulations for the following reasons. The AWI-ESM and Nor-ESM models have LIG

176 simulations with two versions of model. To avoid undue biasing of results, we include only the

177 simulation from the latest version for each model. Additionally, for INM-CM4-8 model, no ocean or

178 sea ice fields were available for download, excluding this model from our analysis. Finally, we

179 exclude the CNRM model in the analysis because apart from using PI instead of LIG GHG

180 concentrations and a short spin-up time, the model also has known issues with its sea-ice model. The

181 model produces much too thin sea ice in September and March compared with observational evidence

182 and the snow layer on the ice is considerably overestimated (Voldoire et al., 2019). As a possible

183 consequence of these issues, the CNRM model is also an outlier in an otherwise highly correlated

184   (inverse) relationship in the models between the LIG-PI albedo change over the Artic sea-ice and the

185   LIG-PI SSAT change over the ice, being the only model that produces a warmer LIG with almost no

186   reduction in albedo (Figure A1). While we consider the CNRM ice model unreliable for this study, we

187   note that the inclusion of the model in our analysis only reduces the correlation coefficients but does

188   not change the overall conclusions.

189

190   We thus analyse the difference between the PI and LIG simulations from eleven models. Out of the

191   eleven simulations of the LIG, seven have 200 years simulation length (data available to download in

192   ESGF), the remaining four are 100 years in length. For PI control runs, we use the last 200 years of PI

193   control run available in ESGF for each model. Details of each model: model denomination, physical

194   core components, horizontal and vertical grid specifications, details on prescribed vs interactive

195   boundary conditions, details of published model description, and LIG simulation length (spin-up and

196   production runs) are contained in (Kageyama et al., 2021). Data was downloaded from the ESGF data

197   node: https://esgf-node.llnl.gov/projects/esgf-llnl/ (last downloaded on 23rd June 2021).

198

199   The spatial distribution of sea ice is usually computed in two ways, by its total area or its extent. The

200   sea ice extent (SIE) is the total area of the Arctic ocean where there is at least 15% ice concentration.

201   The total sea ice area (SIA) is the sum of the sea ice concentration times the area of a grid cell for all

202   cells that contain some sea ice. In this paper, the SIA refers to the SIA of the month of minimum sea

203   ice, as computed by using the climatology of the whole simulation.

204

205   **2.3. Assessing model skill to simulate reconstructions of ΔSSAT**

206   The model skill is quantified using two measures based on 1) the Root Mean Square Error (RMSE) of

207   the modelled SSAT compared to the proxies and 2) the percentage of the 21 proxies for ΔSSAT (in

208   Table 1) for which the model produce a value within the error bars. To assess whether the model

209   match a proxy point, we compute summer mean (June to August) surface air temperatures for every

210   year for the PI and LIG for each model. Climatological summer temperature is the time mean of these

summer temperatures for the entire simulation length. Our calculated model uncertainties on the climatological summer mean temperatures are one standard deviation of summer mean time series for each model. Bilinear interpolation in latitude-longitude space was used to extract values at the proxy locations from the gridded model output. For climatological summer mean temperature, if there is an overlap between proxy SSAT (plus uncertainty) and the simulated SSAT (plus model uncertainty) then, for that location, the result is considered as a match. Similarly, the RMSE error is calculated using the modelled SSAT values averaged over the summer months of the entire simulation length.

3. Results

3.1. Simulated Arctic sea ice distribution

The sea ice distribution in the models have been reported previously in Kageyama et al. (2021) and is included here to make this work self-reliant. For the PI, the model mean value for summer minimum monthly SIA is 6.4 mill. km^2. Due to a lack of direct observations for the PI, the PI model results are compared with 1981 to 2002 satellite observations, keeping in mind that the present day observations are for a climate with a higher atmospheric CO2 level of ~380 ppm, compared to the PI atmospheric CO2 levels of 280 ppm. The modern observed mean minimum SIA is 5.7 mill km^2 (Reynolds et al., 2002). In general, the simulations show a realistic representation of the geographical extent for the summer minimum. More models show a slightly smaller area compared to the present-day observations, however EC-Earth, FGOALS-g3, and GISS170 E2-1-G simulate too much ice (Figure 2). Overestimations appear to be due to too much sea ice being simulated in the Barents-Kara area (FGOALS-g3, GISS-E2-1-G), in the Nordic Seas (EC-Earth, FGOALS-g3) and in Baffin Bay (EC-Earth). Kageyama et al. (2021) also note that MIROC-ES2L performs rather poorly for the PI, with insufficient ice close to the continents. The other models have a relatively close match to the 15% isoline in the NOAA Optimum Interpolation version 2 data (Reynolds et al., 2002; Kageyama et al., 2021).

237 For the LIG, the model output is compared against the LIG sea ice synthesis of Kageyama et al.
238 (2021), which include marine cores collected in the Arctic Ocean, Nordic Seas and northern North
239 Atlantic (Figure 3). These data show that south of 79°N in the Atlantic and Nordic seas the LIG was
240 seasonally ice-free. These southern sea ice records provide quantitative estimates of sea surface
241 parameters based on dinoflagellate cysts (dinocysts). North of 79°N the sea-ice-related records are
242 more difficult to obtain and interpret. A core at 81.5°N brings evidence of summer being probably
243 seasonally ice-free during the LIG from two indicators: dinocysts and IP25/PIP25. However, an
244 anomalous core close by at the northernmost location of 81.9°N, with good chronology, shows IP25-
245 based evidence of substantial (> 75%) sea ice concentration all year round. Other northerly cores do
246 not currently have good enough chronological control to confidently date material of LIG age. All
247 models, except FGOALS, generally tend to match the results from proxies of summertime Arctic sea
248 ice in marine cores with good LIG chronology (Figure 3), apart from the anomalous northernmost
249 core for which the IP25 evidence suggest perennial sea ice (Kageyama et al., 2021). Steinet al. (2017)
250 suggest that PIP25 records obtained from the central Arctic Ocean cores indicating a perennial sea ice
251 cover have to be interpreted cautiously, given that biomarker concentrations are very low to absent, so
252 it is difficult to know how much weight to place on this particular result. Additionally, given Hillaire-
253 Marcel et al. (2017) question the age model of the data from the central Arctic Ocean, thus these IP25
254 data need to be interpreted with some caution. This may mean that all the models tend to have similar
255 problems in simulating Arctic sea ice during the LIG or that the LIG IP25 signal in the Arctic
256 indicates something else. What is clear is that a new approach with other Arctic datasets, such as
257 SSAT, may be needed to make progress on the LIG Arctic sea ice question.
258
259
260
261
262
263
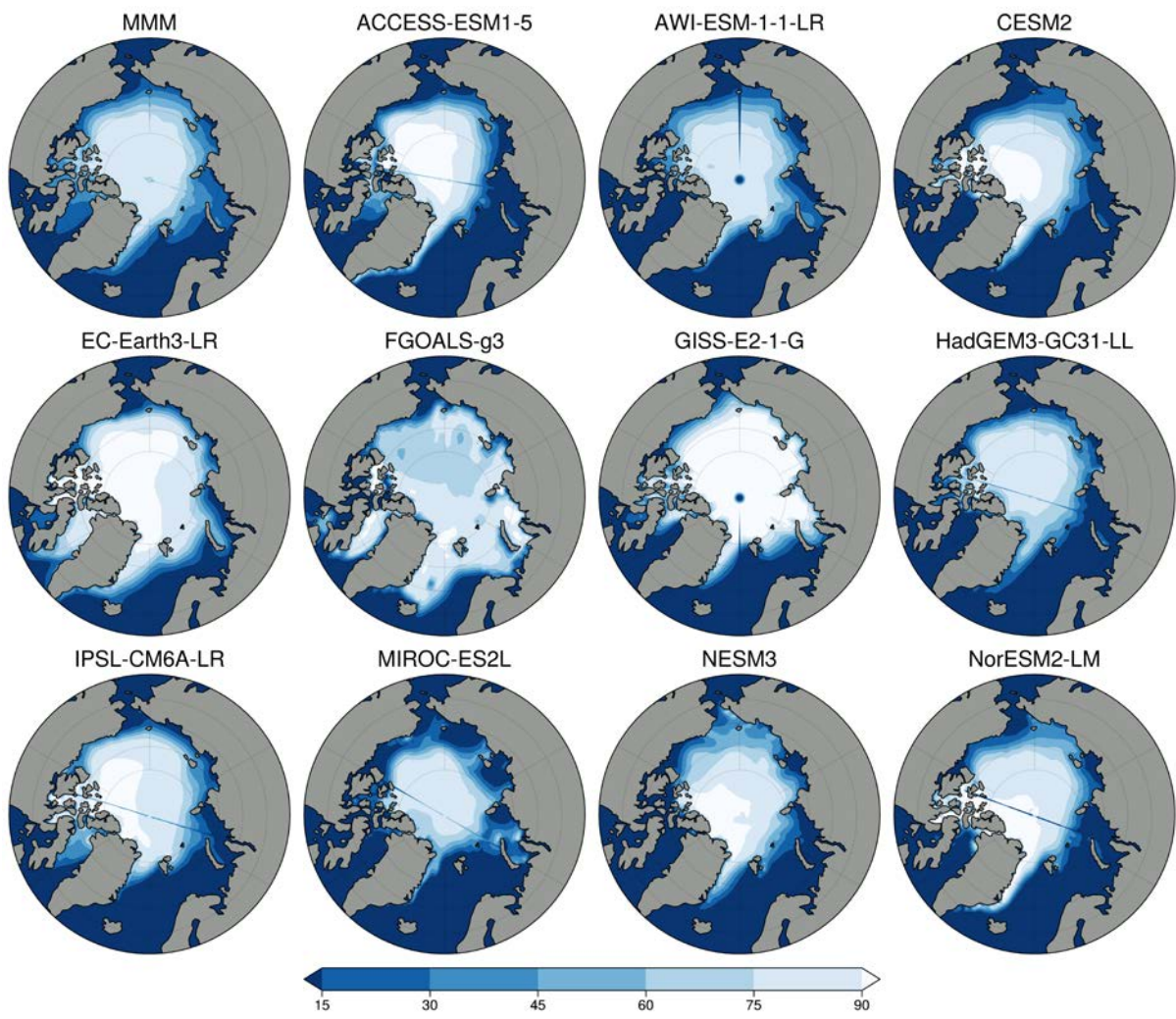
Figure 2: Climatological Minimum PI sea ice concentration maps for each model. The first panel represents the multi model mean (MMM).
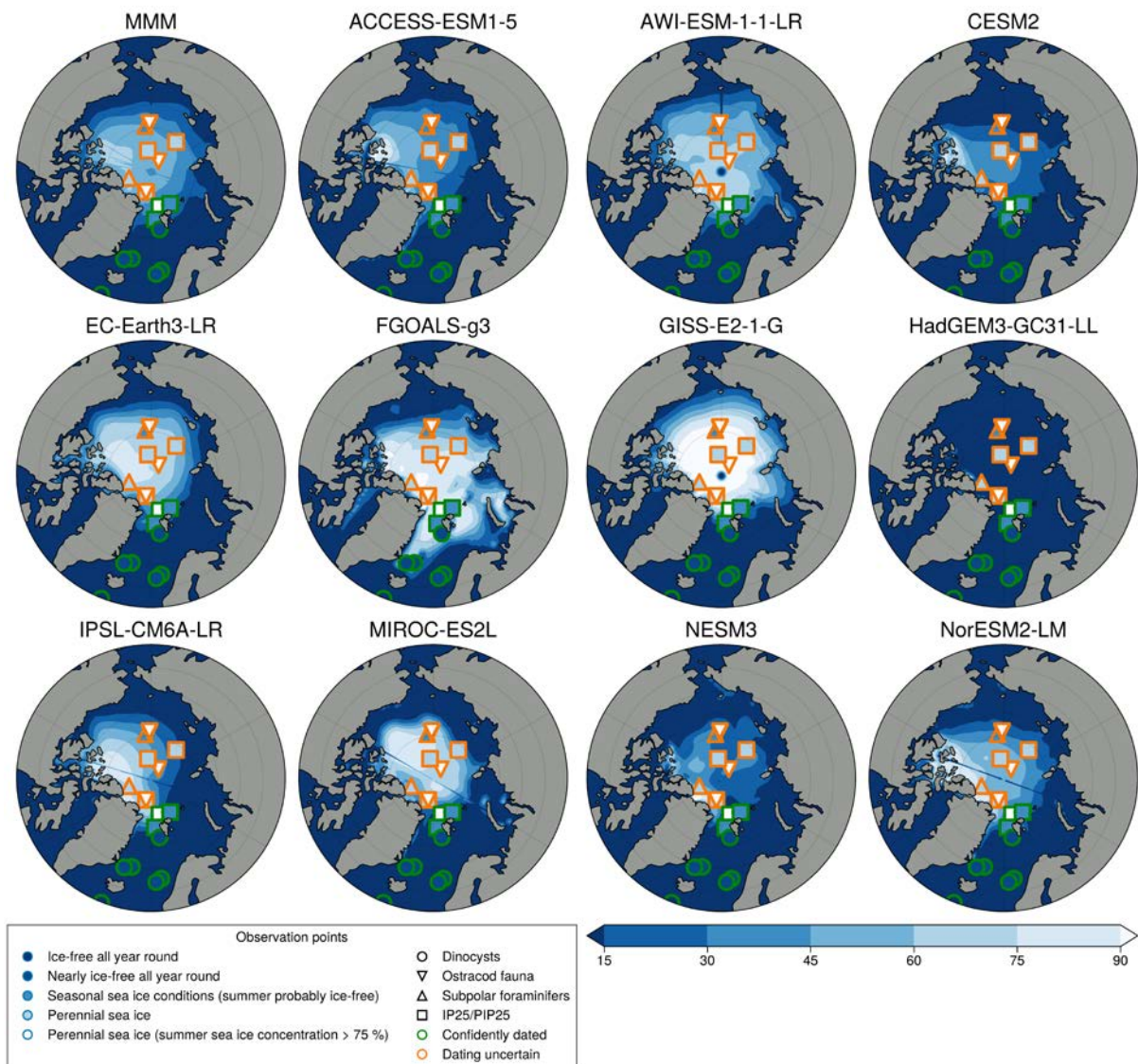
Figure 3: Climatological minimum LIG sea ice concentration maps for each model. Marine core results are from Kageyama et al. (2021): orange outlines indicate that the dating is uncertain; green outlines indicate the datapoint is from the LIG. The first panel represents the multi model mean.

275 For the LIG, there is very little difference between the maximum (wintertime) Arctic SIA and that of
276 the PI (which is 15-16 mill. km^2 between the PI and the LIG in most models), but every model shows
277 a reduction in summer sea ice in the LIG compared to the PI (Table 2). Our model mean LIG
278 summertime Arctic is 2.9 mill. km^2, compared to 6.4 mill. km^2 for the PI, or a 55% PI to LIG
279 decrease. There is large inter-model variability for the LIG SIA during the summer (Figure 4). All
280 models show a larger sea-ice area seasonal amplitude for LIG than for PI, and the range of model SIA
281 is larger for LIG than for PI (Figure A2). The results for individual years show that no model is close
282 to the ice-free threshold fdel summer during their PI simulation (Figure 4) but for the LIG summer
283 SIA, there are three models which are lower than 1 mill. km^2 for at least one summer during the LIG
284 simulation (Figure 4). Of these three, HadGEM3, shows a LIG Arctic Ocean free of sea ice in all
285 summers, *i.e.* its maximum SIE is lower than 1 mill. km^2 in all LIG simulation years. CESM2 and
286 NESM3 show low climatological SIA values (slightly above 2 mill. km^2) in summer for the LIG
287 simulation, and both have at least one year with a SIE minimum which is below 1 mill. km^2, though
288 their average minimum SIE values are just below 3 mill. km^2. Of these low LIG sea ice models,
289 HadGEM3 and CESM2 realistically capture the PI Arctic sea ice seasonal cycle, whilst NESM3
290 overestimates winter ice and the amplitude of the seasonal cycle (Cao et al., 2018).

291

292

293 *Table 2: The minimum climatological sea ice area for the PI and the LIG, changes, and the*
294 *associated ΔSSAT anomalies. Percentage reductions are calculated from PI minimum SIA for each*
295 *model.*

MODEL	SIA PI	SIA LIG	ΔSIA	SIA	ΔSSAT
(units)	(mill. km^2)	(mill. km^2)	(mill. km^2)	(% loss)	(K)
MMM	6.36	2.93	-3.43	53.87	3.6±1.3
ACCESS-ESM1-5	5.48	2.39	-3.09	56.44	2.6±1
AWI-ESM-1-1-LR	5.37	3.76	-1.61	29.99	1.7±1.1
CESM2	5.31	1.62	-3.69	69.54	3.3±1
EC-Earth3-LR	8.86	3.65	-5.21	58.84	5.7±2.6

FGOALS-g3	8.83	5.55	-3.29	37.19	4.8±1.5
GISS-E2-1-G	8.87	5.54	-3.32	37.47	3.4±1.4
HadGEM3-GC31-LL	5.21	0.13	-5.07	97.48	4.9±1.2
IPSL-CM6A-LR	6.42	2.46	-3.96	61.74	4.4±1.2
MIROC-ES2L	4.20	2.79	-1.41	33.66	2.1 ± 0.6
NESM3	5.50	1.64	-3.86	70.14	3 ±0.9
NorESM2-LM	5.92	2.75	-3.17	53.52	3.6±1.1

296
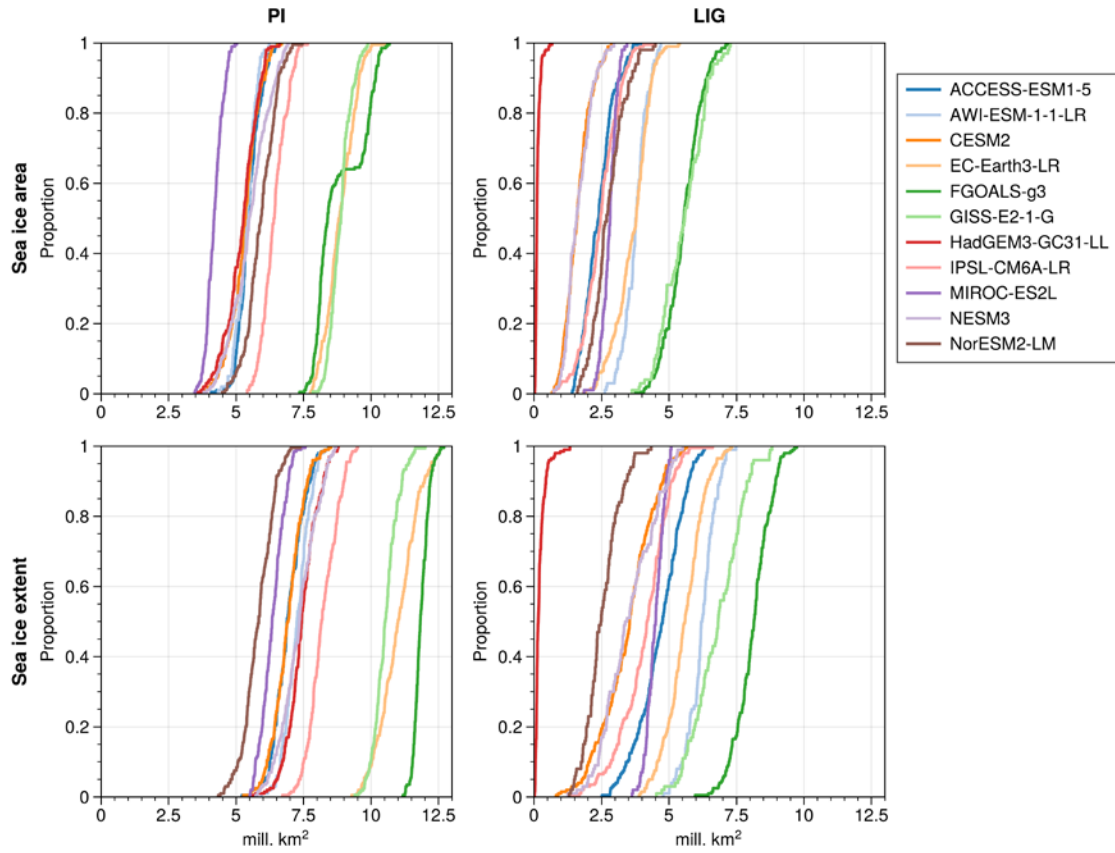
Figure 4: Cumulative distribution of minimum SIA of individual years in LIG and PI simulations, i.e SIA versus proportion of years which fall below the corresponding SIA value. HadGEM3 has minimum SIA below 1 mill km² for all years in LIG runs. CESM2 has 6.5%, and NESM3 8%, LIG years with SIA below 1 mill km². Lower Panels are same but for SIE.

3.2. Estimating ΔSIA from model skill to simulate ΔSSAT

We first investigate whether there is a relationship between how well models match proxy ΔSSAT and the magnitude of SIA reduction that they simulate for the LIG. A visual comparison of modelled ΔSSAT and proxy estimates for ΔSSAT is also shown in Figure 5. As described in Section 2, two different approaches are used to quantify the skill of the models to simulate ΔSSAT, based on 1) the RMSE of the model-data ΔSSAT at the proxy record locations and 2) the percentage ΔSSAT proxies

303   that the model can correctly match, within model and data error. Here the focus is on quantifying

304   model skill across all data records, but for reference, the model-versus-proxy ΔSSAT for each

305   location is provided for each model individually in Figure A3. The RMSE skill estimate and the

306   percentage match estimate provide very similar indications of which models have good skill to

307   reproduce proxy ΔSSAT. The five models with the lowest RMSE also have the highest percentage

308   match and the two models with the highest RMSE have the lowest percentage match (Figure 6). Both

309   approaches show that the models with better skill to simulate ΔSSAT have a high absolute ΔSIA. The

310   only outlier is EC-Earth, which has an average skill (6th best model of 11) but a high SIA reduction at

311   the LIG. This occurs because the EC-Earth PI simulation has an excessive SIA, more than 3 million

312   km^2 compared with present day estimations; this enables it to have a large ΔSIA value, whilst likely

313   retaining too much LIG SIA. Quantitively there is a correlation of r=-0.65 (p=0.03) between the

314   magnitude of ΔSIA and the RMSE, and a correlation with r=0.67 (p=0.02) between the magnitude of

315   ΔSIA and the percentage match of the model (Figure 6). Given that the SIA reduction from the PI to

316   the LIG could be dependent on the starting SIA at the PI, we repeat the analysis for percentage SIA

317   loss from the PI (rather than absolute SIA loss) and find that is correlates similarly to the model skill

318   to reproduce ΔSSAT (Figure A4).

319

320

321
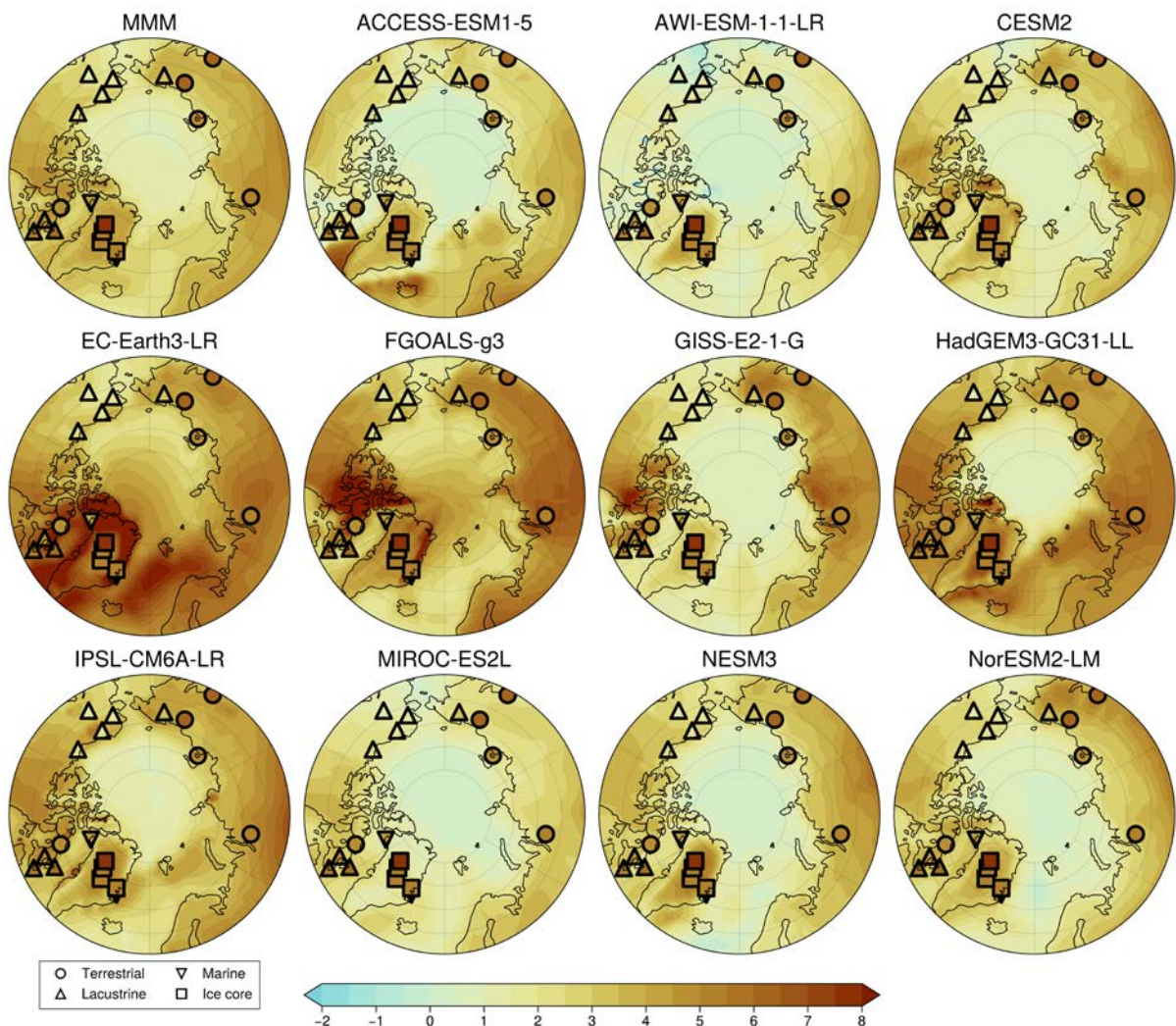
Figure 5: Summertime surface air temperature (SSAT) anomaly (LIG - PI) maps for each model overlain by reconstructed summer temperature anomalies. Proxies are detailed in Table 1 and Guarino et al. (2020b); colours are the same as used for the underlying model data. The first panel represents the multi model mean.

326
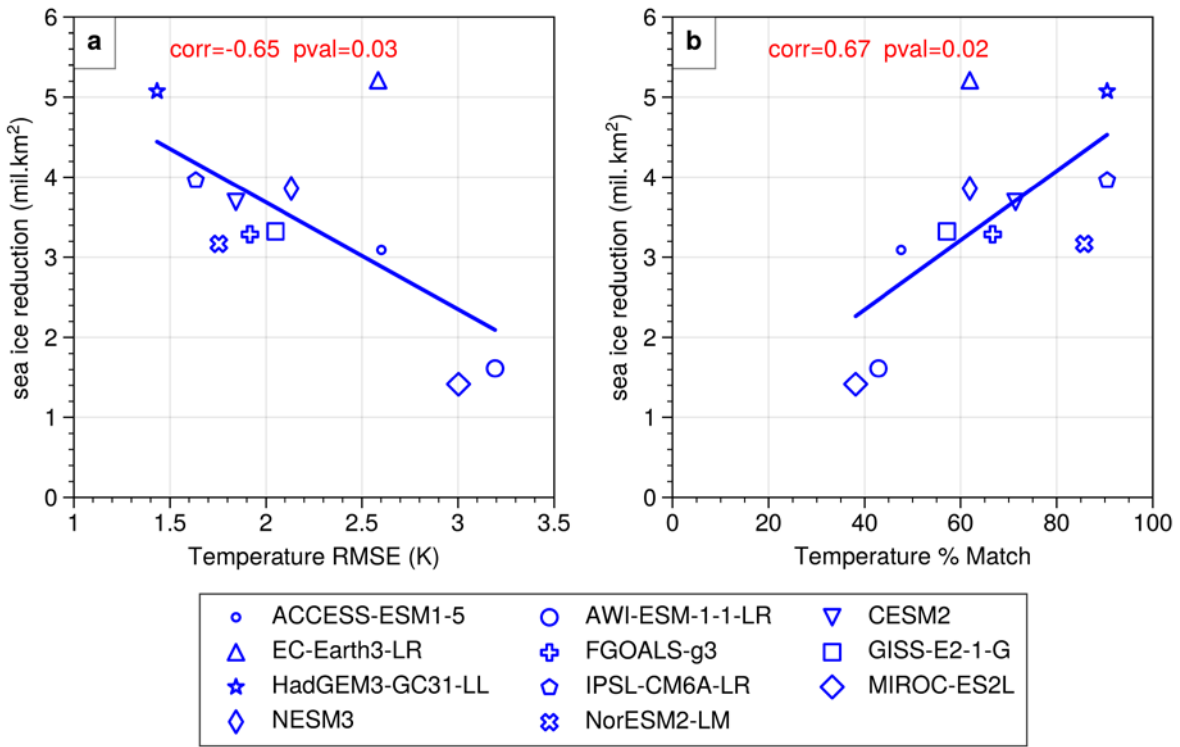
327

328

329 *Figure 6: Modelled magnitude of ΔSIA versus model skill to simulate proxy ΔSSAT. a) The modelled*
330 *magnitude of ΔSIA is scattered against the RMS error of the modelled ΔSSAT compared to the proxy*
331 *ΔSSAT for the 21 data locations. b) The modelled magnitude of ΔSIA scattered against the percentage*
332 *of ΔSSAT data points that the model can match (see methods).*

333

334   In general, where models have a closer match with the ΔSSAT, they have a higher absolute ΔSIA, as

335   well as a larger percentage reduction of SIA from the PI. We thus look at our best performing models

336   for an indication of true LIG Arctic sea ice reduction. The four models with the best agreement of

337   ΔSSAT to proxies are in order of skill; HadGEM3, IPSL, NORESM2, and CESM2. The top two

338   performing models simulate an average SIA loss of 4.5 mill. km^2 from an average starting PI SIA of

339   5.8 mill. km^2 to a final LIG SIA of 1.3 mill. km^2, which equates to a percentage SIA loss of 79%.

340   Including also the two next-best performing models in the average results in an average SIA loss of

341   4.0 mill. km^2 to a final LIG SIA of 1.7 mill. km^2 from an average starting PI SIA of 5.7 mill. km^2,

342   which equates to a percentage SIA loss of 71%.

343

344   The question arises as to why there is a linear relationship between model skill to simulate Arctic

345   ΔSSAT and SIA reduction. One possibility is that the mean proxy ΔSSAT of 4.5 K is higher than

346   what most models produce, and that the warmer models are thus closer to the proxies and also more

347   likely to reduce sea ice. In the next section, this question is addressed by investigating whether ΔSIA

348   is closely related to ΔSSAT itself.

349

350   **3.3. Estimating ΔSIA from the modelled ΔSIA-ΔSSAT relationship and proxy ΔSSAT**

351   Here we investigate whether the models suggest a linear relationship between ΔSSAT and ΔSIA, and

352   if so, exploit that together with proxy ΔSSAT to estimate the most likely (true) value for ΔSIA. We

353   first calculate the mean ΔSSAT in the model at all 21 proxy data locations and compare it to the

354   magnitude of ΔSIA in each model (Figure 7a). The two are well correlated with r=0.86 (p=0.001) and

355   the regression equation provide a dependence of ΔSIA on ΔSSAT. Using this relation, the

356   reconstructed mean ΔSSAT at the proxy locations(4.5±1.7) points to a SIA reduction of 4.2±1.4 mill.

357   km^2 from the PI. This constitutes about 74% reduction from the present day observation of 5.7 mill.

358   km^2, which is also the average SIA for the PI in the two most skilful models identified in the previous

359   section. Using this value for the PI sea ice, suggests remaining minimum of 1.5 mill. km^2 of sea ice

360   during the LIG summer. An average LIG minimum of 1.5 mill. km^2 implies that some LIG summers

361   must have been ice-free (below 1 mill. km^2 in SIE) but that most summers would have had a small

362   amount of sea ice.
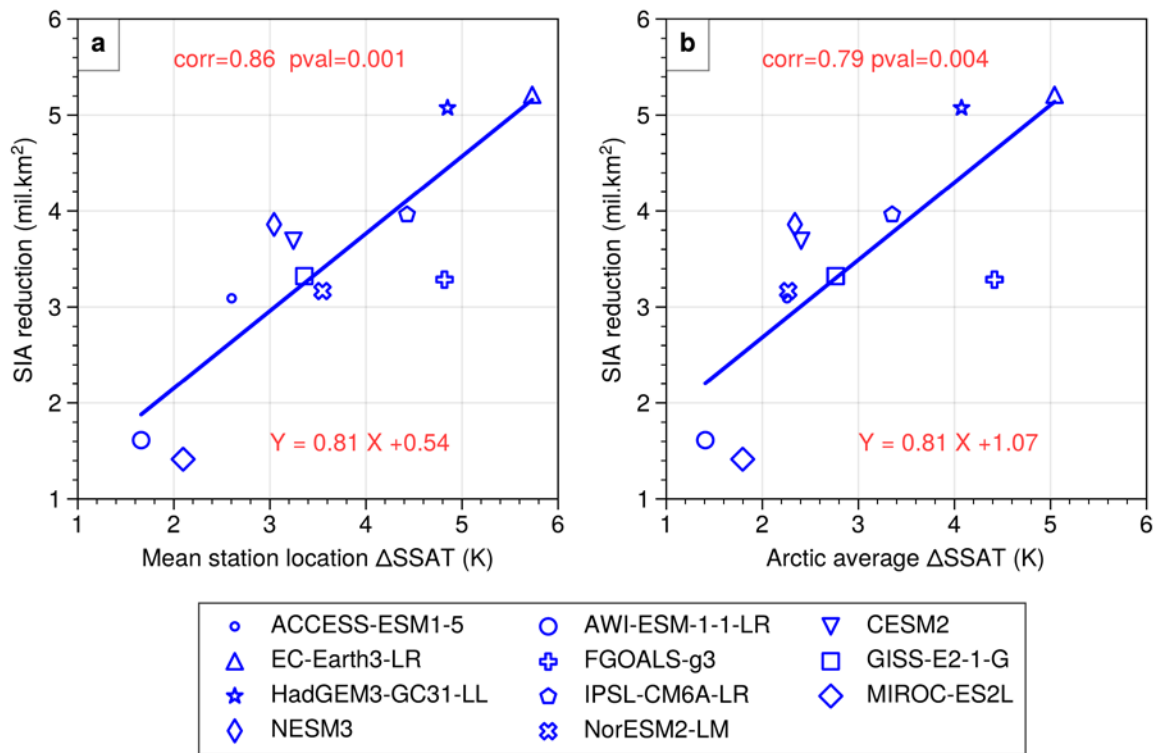
Figure 7: Modelled magnitude of ΔSIA versus modelled ΔSSAT for the Arctic. a) The modelled ΔSIA is scattered against mean modelled ΔSSAT at the 21 data locations. b) The modelled ΔSIA is scattered against the mean modelled ΔSSAT averaged over the Arctic north of 60°N.

The ΔSSAT relationship to ΔSIA has so far been computed using the mean ΔSSAT at the locations of the data. To test whether this method would also work for the Arctic in general, the ΔSSAT is next averaged over the whole Arctic north of 60°N and compared with ΔSIA (Figure 7b). The correlation between ΔSSAT and ΔSIA is a somewhat reduced when calculating ΔSSAT across the whole Arctic, though it is still highly significant (r=0.79, p=0.004). An estimate for proxy-based Arctic-wide ΔSSAT can be derived by applying the close relationship between Arctic ΔSSAT and station ΔSSAT in the models (Figure 8, r=0.97, p <0.001). Inserting the ΔSSAT averaged over all proxy-records, of 4.5±1.7 K, in the regression equation in Figure 8, gives an estimate for proxy-based Arctic-wide

376   ΔSSAT of 3.7±1.5 K. Applying the regression equation in Figure 7b and using this estimate for

377   Arctic-wide ΔSSAT suggests a PI to LIG sea ice reduction of 4.1±1.2 mill. km^2, which is very similar

378   to the estimate derived from the station data alone (of 4.2±1.4 mill. km^2).

379
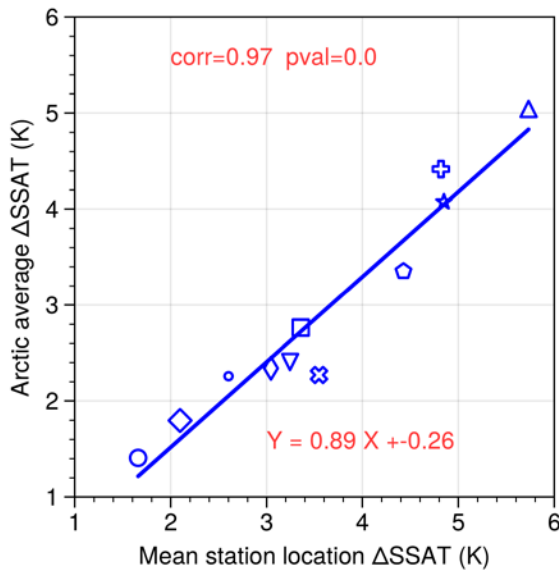
392   Figure 8: Modelled Arctic-wide ΔSSAT versus modelled mean ΔSSAT at the data locations for the 11

393   models. The markers for each model are same as in Figure 7

394

4. Discussion and conclusions

396   As discussed in the introduction, neither proxies nor modelling results alone allow currently for a

397   convincing estimate of the Arctic sea ice reduction at the LIG. Here we apply a joint approach to

398   make progress. We deduce how much sea ice was reduced during the LIG, using 11 of the most recent

399   CMIP6-PMIP4 LIG model simulations and proxy observations of summer air temperature changes.

400   The reduction of sea ice from the PI to the LIG in the models range from 30% to 96% with an average

401   of 55%. No model is close to the ice-free threshold, of maximum SIE lower than 1 mill. km^2, for any

402   model year-summer during their PI simulation. During the LIG, the HadGEM3 model is the only one

403   that has an Arctic Ocean free of sea ice in all summers, although CESM2 and NESM3 show SIA

404   values of around 2 mill. km^2, in association with intermittently ice-free conditions. We found that

405   larger LIG SIA reduction from the PI is related to greater SSAT warming, the two being correlated

406   with r=0.86 across the models. In particular, 8 out of 11 models are able to match, within uncertainty,

407   the average PI to LIG summertime Arctic warming of 4.5 ± 1.7 K as recorded by surface temperature

408   proxies. This magnitude of warming was difficult to reach with previous generations of LIG models.

409   Among the models, two of them capture the magnitude of the observed dSSAT in more than 60% of

410   the total proxy locations. These models simulate an average LIG sea ice area of 1.3 mill. km2 which is

411   a 4.5 mill. km2 (or 79%) reduction from their PI values.

412

413   We find that the good match between the (ice-free) HadGEM3 and the Guarino et al. (2020b) summer

414   Arctic temperature dataset is not unique. However, we find that it is not random either and that there

415   is a correlation between model skill to match the ΔSSAT and the reduction of SIA from the PI to the

416   LIG (both when using an RMSE skill test and when using a best-match skill test). The two most

417   skilful models simulate an average LIG sea ice area of 1.3 mill. km^2 which is a 4.5 mill. km^2 or 79%

418   reduction from their PI values. Whilst we cannot assume all model error ΔSSAT is attributable to

419   ΔSIA, it is reasonable to assume that the better performing models for ΔSSAT are also better at

420   simulating ΔSIA, because of the close relationship between warming and sea ice loss.

421

422   Some of the proxies are more difficult for the models to simulate (Figure 9 and Figure A3). In

423   particular, it appears that the Greenland ice core SSAT value from NEEM of +8 (proxy record 21 in

424   Table 1 Figure 9) is higher than any model simulates; though with a ±4 K uncertainty it is

425   nevertheless matched by some models. Terrestrial proxies three and six, with SSAT values of +6.4 K

426   are also only rarely matched. Further work on the observational side would be useful. These LIG

427   SSAT proxy reconstructions were used in the IPCC (2013) report and by Guarino et al. (2020b); and

428   were previously published by IPCC (2013); CAPE members (2006); Kaspar et al. (2005); Capron et

429   al. (2017). Thus, this dataset should ideally be improved. One start point for this would be adding

430   uncertainties to the (nine) sites which do not currently have these numbers.

431

432
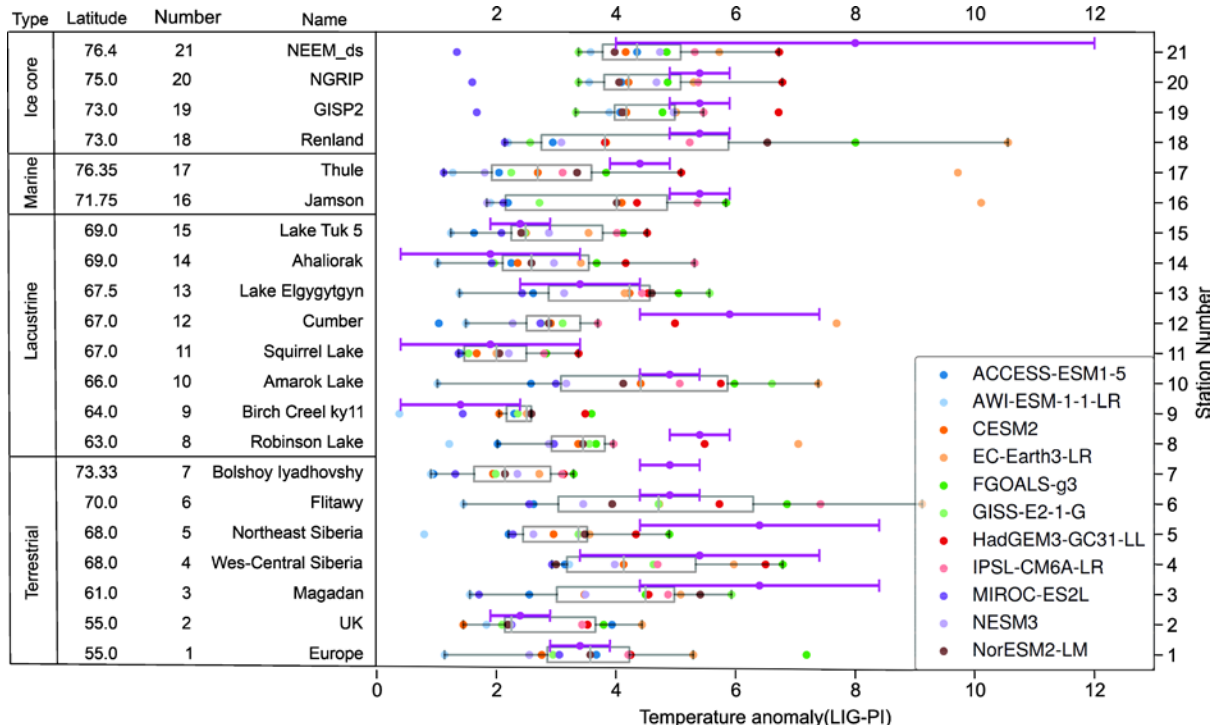
Figure 9: Proxy ΔSSAT (violet dots and uncertainty bars) and simulated ΔSSAT for all models (coloured dots) for each proxy record location (rows). Grey boxes extend from the 25th to the 75th percentile of each locations distribution of simulated values and the vertical lines represent the median.

437

438   The correlation between model skill to simulate ΔSSAT and the magnitude of ΔSIA is convincing (r=

439   0.66 and p= 0.003 on average for the two skill tests). However, the two quantities are not

440   straightforward to relate through a dynamical process. On the other hand, it is well known that there is

441   a positive feedback between Arctic temperature and Arctic sea-ice, with warmer temperatures more

442   likely to melt sea ice, and less sea ice producing a smaller albedo to incoming solar radiation and so

443   less cooling from solar reflection. Figure A6 shows the relationship between summer surface air

444   temperature anomalies versus September sea ice area from the observational estimates for the period

445   from 1979-2020. In present time, the relationship between minimum SIA and summer SAT is 1.32

446   mil. Km^2 decrease per 1K temperature rise. This dynamic relationship is also evident in LIG

447   simulations, with a strong correlation of r=0.86 between the magnitude of ΔSIA and ΔSSAT across

448   all the models and the intermodel relationship suggests sea ice decrease of 1.9 mill km^2 per 1K

449   temperature rise (from the regression equation in Figure 7b). The reconstructed ΔSSAT from

450   proxies, of 4.5 ±1.7 K, is larger than most models simulate, so the models that match the ΔSSAT most

451   closely would be the models with a larger ΔSSAT than average and thus also a larger ΔSIA. The only

452   model that has a large SIA reduction and not a good skill to match SSAT is EC-Earth, which features

453   a PI simulation with far too much sea ice, which allows an excessive LIG to PI Arctic warming. An

454   additional result of our study is that the mean ΔSSAT at the proxy locations is strongly correlated to

455   Arctic-wide ΔSSAT north of 60°N in the models (r=0.97). Applying the regression relation between

456   the two, implies that the mean ΔSSAT at the proxy locations, of 4.5±1.7 K, is equivalent to an Arctic-

457   wide warming at the LIG of 3.7±1.5 K. This is thus a more representative value for the Arctic

458   warming at the LIG, than using the simpler proxy-location average.

459

460   The strong linear correlation between the magnitude of ΔSIA and ΔSSAT is applied to the proxy-

461   reconstructed ΔSSAT to give an estimate of the reduction of SIA from the PI to LIG of 4.2±1.4 mill.

462   km^2, similar to that derived from our "best skill" approach. A similar value of 4.1±1.2 mill. km^2 is

463   obtained when extrapolating the method to Arctic-wide ΔSSAT north of 60°N. The models and data

464   have uncertainties, and the regressions applied are not between perfectly correlated quantities.

465   However, it is clear from both applied methods (each with two variants) that proxy-reconstructed

466   ΔSSAT, in combination with the model output, implies a larger sea ice reduction than the

467   climatological multi-model mean of 55%. It suggests a LIG SIA of ~1.5 mill. km^2, which is consistent

468   with intermittently ice-free summers – but with (low ice area) ice-present summers likely exceeding

469   the number of ice-free years.

470

471   Whilst we have focussed here on the Arctic SIA response to LIG insolation forcing, Kageyama et al.

472   (2021) found that the models that respond strongly to LIG insolation forcing also respond strongly to

473   CO_2 forcing. Indeed the models with the weakest response for the LIG had the weakest response to

474   the CO_2 forcing. This suggests that our assessment here of model skill against Arctic SIA and SSAT

475 change can also help, to some extent, ascertain the models which have a better Arctic SIA and SSAT

476 response to CO2 forcing. Overall the results presented in this study suggest that: (i) the fully-ice free

477 HadGEM3 model is somewhat too sensitive to forcing; it loses summer sea ice too readily during the

478 LIG; and (ii) most other PMIP4 models are insufficiently sensitive - these models do not lose enough

479 sea ice.

480

481 *Code availability.* Python code used to produce the manuscript plots is available on request from the

482 authors.

483

484 *Data availability.* The summer air temperature dataset is available at https://data.bas.ac.uk/full-

485 record.php?id=GB/NERC/BAS/PDC/01593. All model data is available from the ESGF data node:

486 https://esgf-node.llnl.gov/projects/esgf-llnl/.

487

488

489

490

491 **Appendix**

492 **A1. Inter-model differences in LIG Sea ice simulation**

493

494 Sea ice formation and melting can be affected by a large number of factors inherent to the atmosphere

495 and the ocean dynamics, alongside the representation of sea ice itself within the model (i.e. the type of

496 sea ice scheme used). In coupled models it can therefore be difficult to identify the causes of this

497 coupled behavior (Kagayama et al. 2021, Sicard et al,2022). Nevertheless Kagayama et al. (2021;

498 Section 4), alongside Diamond et al. (2021) address the question of what drives model differences in

499 summertime LIG sea ice. In summary:

500 1. All PMIP4-LIG simulations show a major loss of summertime Arctic sea ice between the PI and

501 LIG.

502   2. Across all models, there is an increased downward short-wave flux in spring due to the imposed

503   insolation forcing and a decreased upward short-wave flux in summer, related to the decrease of the

504   albedo due to the smaller sea ice cover. Differences between the model results are due to a difference

505   in phasing of the downward and upward shortwave radiation anomalies.

506   3. The sea ice albedo feedback is most effective in HadGEM3. It is also the only model in which the

507   anomalies in downward and upward shortwave radiation are exactly in phase.

508   4. The CESM2 and HadGEM3 models (which both simulate significant sea ice loss) exhibit an

509   Atlantic Meridional Overturning Circulation (AMOC) that is almost unchanged between PI and LIG,

510   while in the IPSLCM6 model (with moderate sea ice loss) the AMOC weakens. This implies that a

511   reduced northward oceanic heat transport could reduce sea ice loss in the Central Arctic in some

512   models.

513   5. The two models (HadGEM3 and CESM2) which had the lowest sea ice loss contain explicit melt

514   pond schemes, which impact the albedo feedback in these models. Diamond et al. (2021) show that

515   that the summer ice melt in HadGEM3 is predominantly driven by thermodynamic

516   processes and those thermodynamic processes are significantly impacted by melt ponds.

517

518

519   **Appendix Figures**

520

521
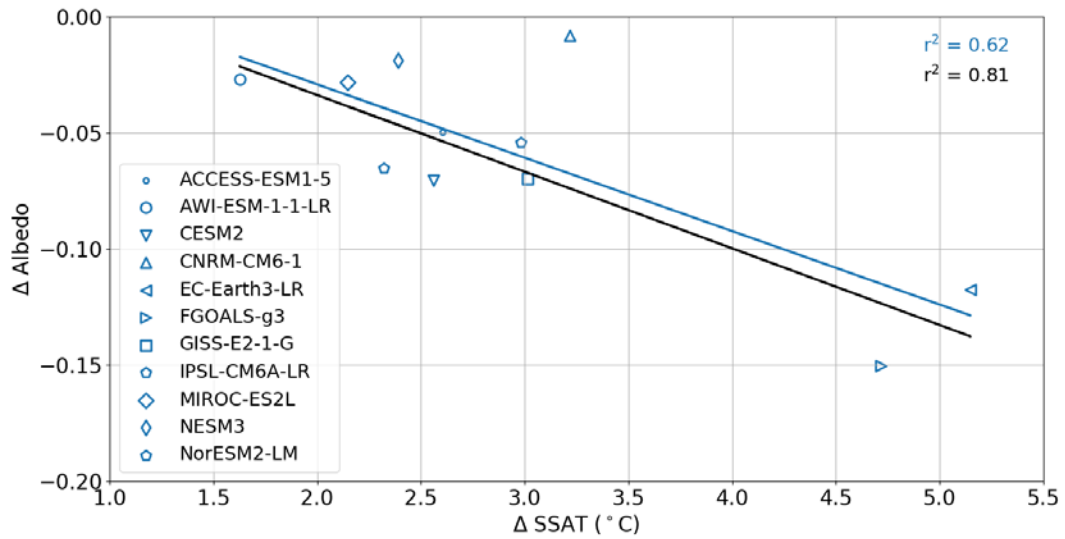
522

523

524   Figure A1. LIG-PI change in albedo over Arctic sea-ice as a function of LIG-PI change in SSAT (°C)

525   over the ice. The r^2 values and the linear fit lines are for the models including CNRM (blue) and

526   excluding CNRM (black). The CNRM model (upside triangle) is an outlier that influences the

527   strength rather than the nature of the correlation.
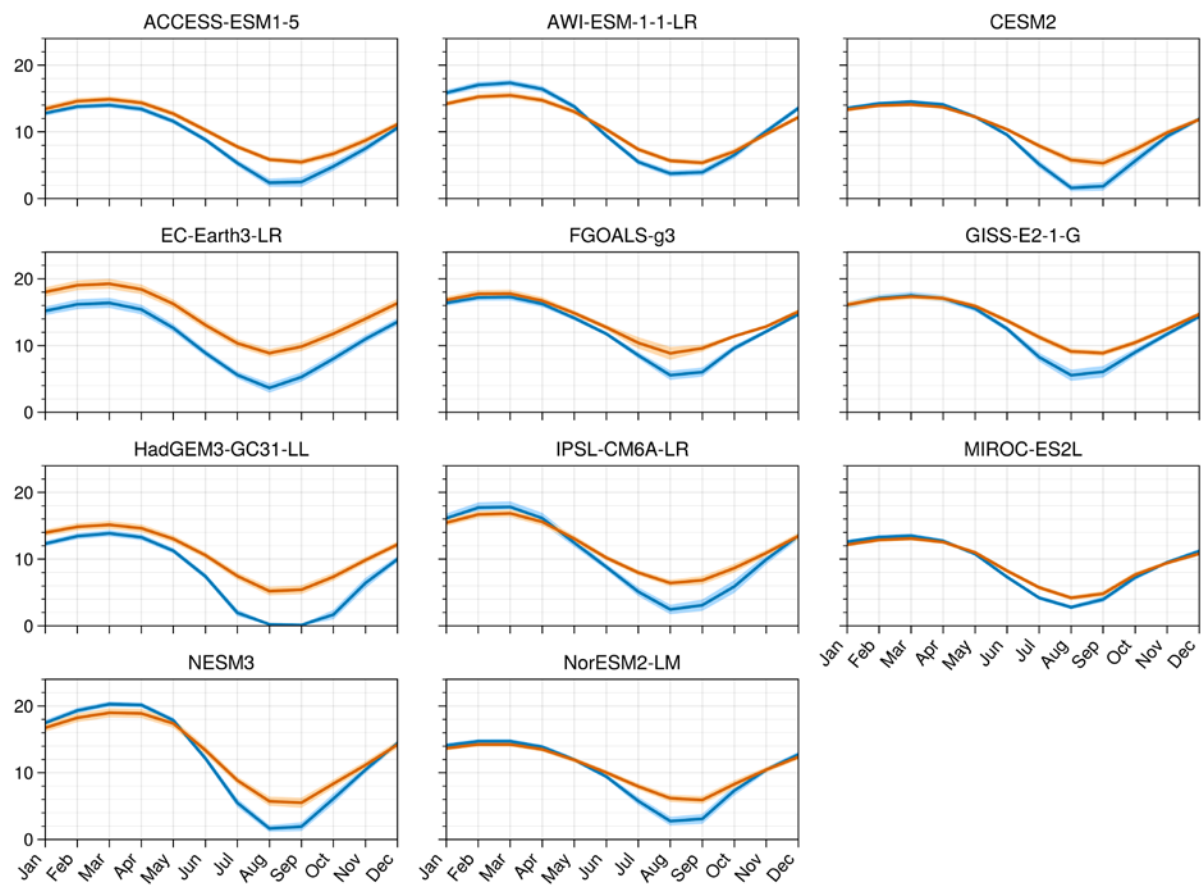
528

529   Figure A2. Sea ice area climatological seasonal cycle for each model.

530
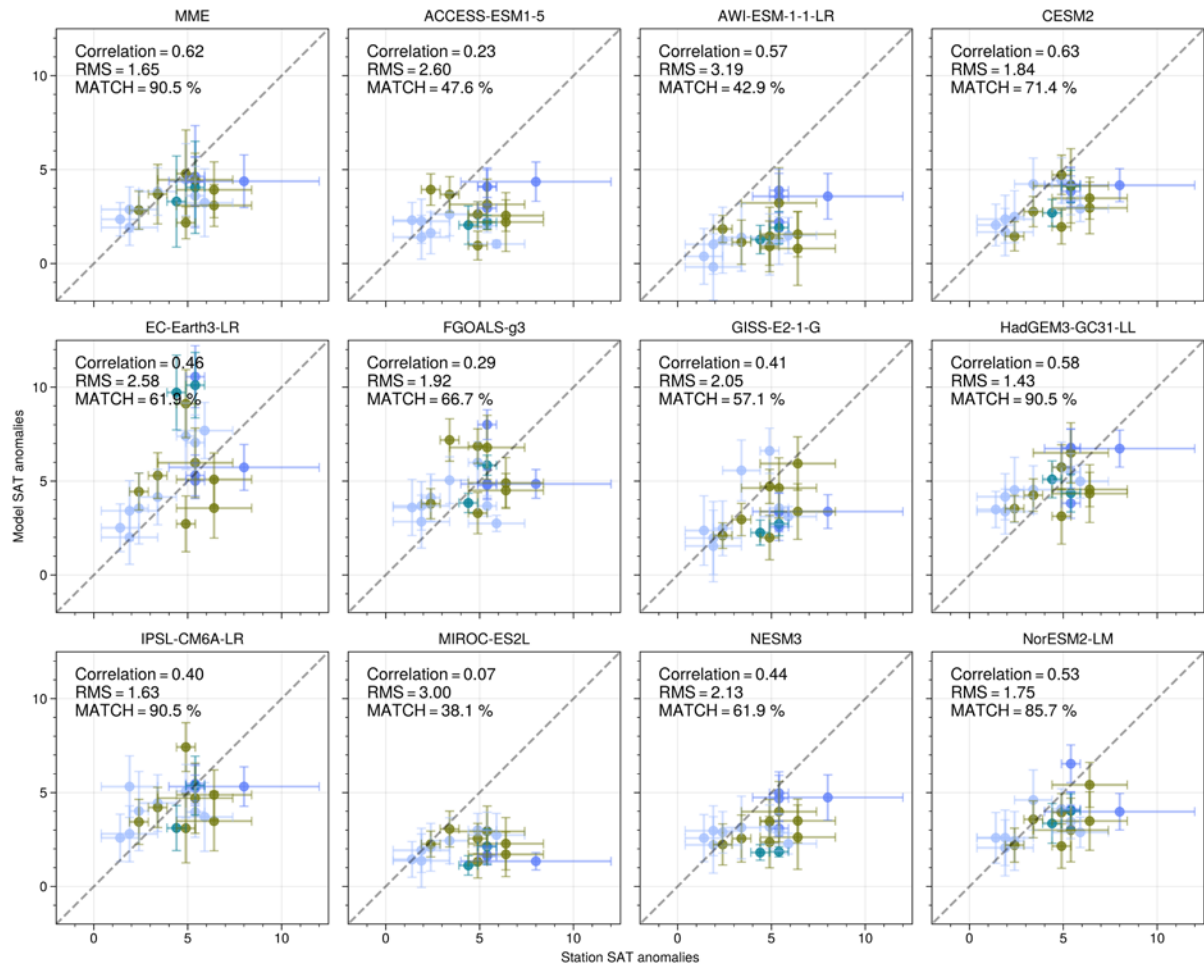
Figure A3. Modelled ΔSSAT versus proxy ΔSSAT. The scatter points show model data versus reconstuctions for each proxy location. Error-bars represent one standard deviation on either side of the proxy estimate. The correlation coefficients, between X and Y, RMSE and percentage matches with proxy data for each model are indicated in each panel.

535

536
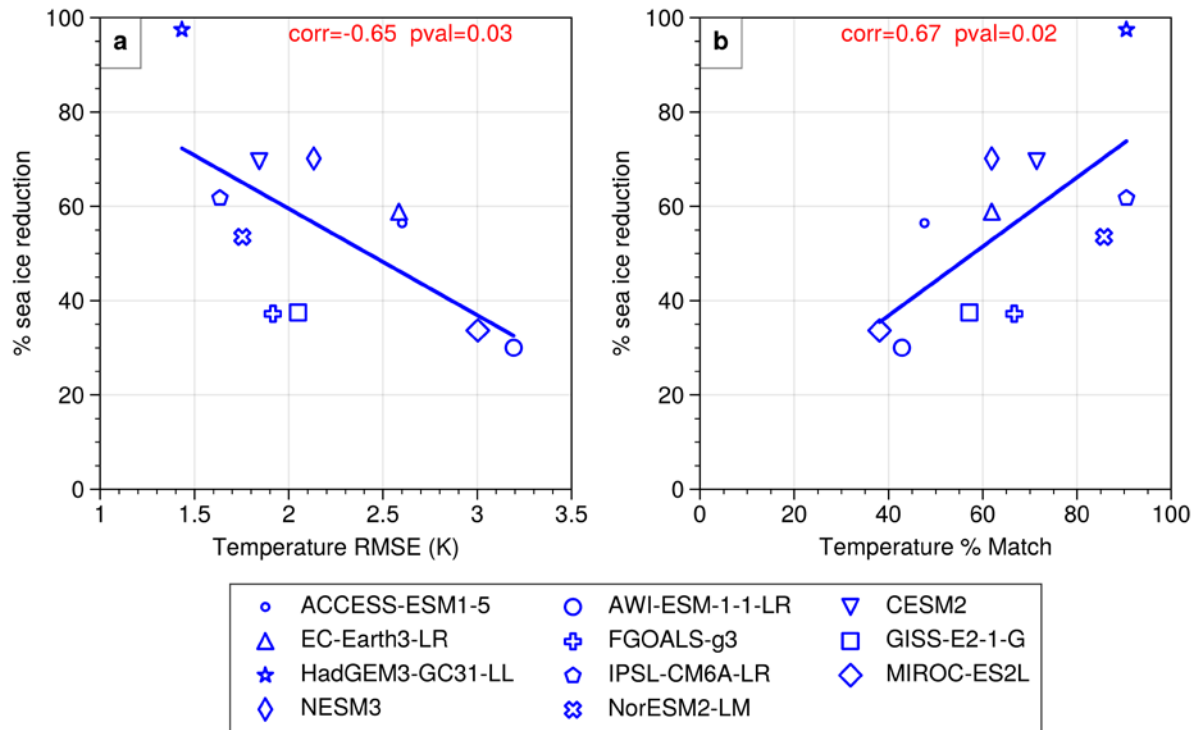
Figure A4: Modelled % sea ice area reduction from the LIG to the PI versus model skill to simulate proxy ΔSSAT. a) The modelled %SIA reduction is scattered against the RMSE of the modelled ΔSSAT compared to the proxy ΔSSAT for the 21 data locations. b) The modelled % SIA reduction scattered against the percentage of ΔSSAT data points that the model can match (see methods).
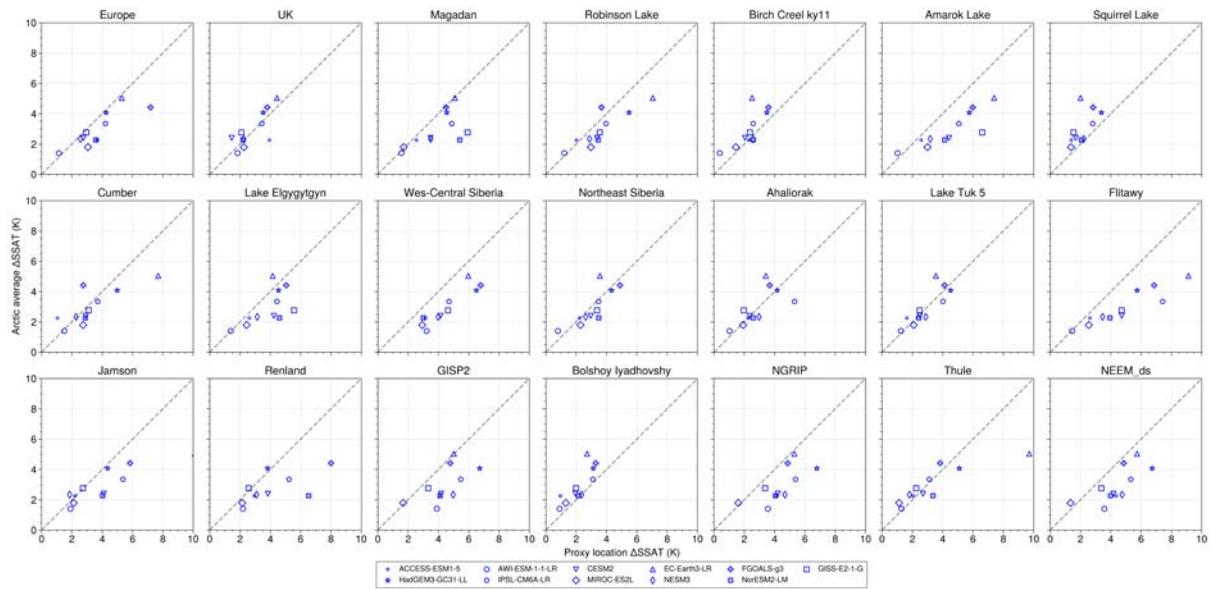
541   Figure A5. Scatter Plot for climatological ΔSSAT at each proxy location versus climatological

542   ΔSSAT averaged north of 60°N in each model

543

544
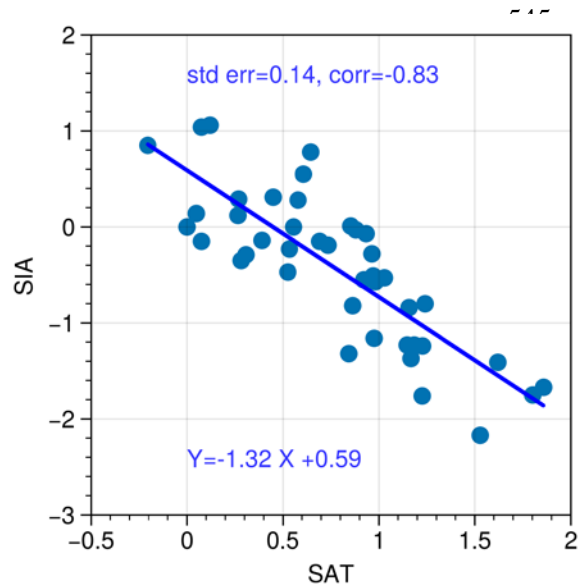
557

558 Figure A6:- Scatter plot of SAT versus SIA for current period. JJA surface air temperature versus NH

559 September Sea ice area for each year from 1979-2020. Anomalies computed from year 1979 values.

560 SIA is from NSIDC (https://nsidc.org/data/g02135/versions/3) and Air temperature (area averaged

561 north of 60°N) is from ERA5 reanalysis (Hersbach et al. 2020).

562

563

564 *Author contributions*. LCS planned and wrote the original draft. RS analysed model results and

565 prepared the figures. Figure 1 which was prepared by IVM. AdB wrote the second draft. MS

566 undertook additional analysis, checks and researched particular model results. All authors contributed

567 to the final text.

568

569 *Competing interests.* The authors have no competing interests.

570

571 *Acknowledgements.* LCS and RS acknowledge the financial support of NERC research grant

572 NE/P013279/1 and NE/P009271/1. LCS and IVM have received funding from the European Union's

573 Horizon 2020 research and innovation programme under grant agreement No 820970. AdB and MS

574 were supported by Swedish Research Council grant 2020-04791. This work used the ARCHER UK

575 National Supercomputing Service (http://www.archer.ac.uk) and the JASMIN analysis platform

576 (https://www.ceda.ac.uk/services/jasmin/).

References

Bartlein, P. J. and Shafer, S. L.: Paleo calendar-effect adjustments in time-slice and transient climate-model simulations (PaleoCalAdjust v1.0): Impact and strategies for data analysis, Geoscientific Model Development, 12, 3889–3913, 2019.

Belt, S.: Source-specific biomarkers as proxies for Arctic and Antarctic sea ice, Org. Geochem., 125, 277–298, https://doi.org/10.1016/j.orggeochem.2018.10.002, 2018.

Berger, A. and Loutre, M.-F.: Insolation values for the climate of the last 10 million years, Quaternary Science Reviews, 10, 297–317, 1991.

Bracegirdle, T. J., Colleoni, F., Abram, N. J., Bertler, N. A. N., Dixon, D. A., England, M., Favier, V., Fogwill, C. J., Fyfe, J. C., Goodwin, I., Goosse, H., Hobbs, W., Jones, J. M., Keller, E. D., Khan, A. L., Phipps, S. J., Raphael, M. N., Russell, J., Sime, L., Thomas, E. R., van den Broeke, M. R., and Wainer, I.: Back to the Future: Using Long-Term Observational and Paleo-Proxy Reconstructions to Improve Model Projections of Antarctic Climate, Geosciences, 9, https://doi.org/10.3390/geosciences9060255, 2019.

Cao, J., Wang, B., Yang, Y.-M., Ma, L., Li, J., Sun, B., Bao, Y., He, J., Zhou, X., and Wu, L.: The NUIST Earth System Model (NESM) version 3: description and preliminary evaluation, Geoscientific Model Development, 11, 2975–2993, https://doi.org/10.5194/gmd-11-2975-2018, 2018.

CAPE members: Last Interglacial Arctic warmth confirms polar amplification of climate change, Quaternary Science Reviews, 25, 1383– 1400, 2006.

Capron, E., Govin, A., Stone, E. J., Masson-Delmotte, V., Mulitza, S., Otto-Bliesner, B., Rasmussen, T. L., Sime, L. C., Waelbroeck, C., and Wolff, E. W.: Temporal and spatial structure of multi-millennial temperature changes at high latitudes during the Last Interglacial, Quaternary Science Reviews, 103, 116–133, https://doi.org/10.1016/j.quascirev.2014.08.018, 2014.

Capron, E., Govin, A., Feng, R., Otto-Bliesner, B. L., and Wolff, E. W.: Critical evaluation of climate syntheses to benchmark CMIP6/PMIP4 127 ka Last Interglacial simulations in the high-latitude regions, Quaternary Science Reviews, 168, 137–150, 2017.

603 Diamond, R., Sime, L. C., Schroeder, D., and Guarino, M.-V.: The contribution of melt ponds to
604 enhanced Arctic sea-ice melt during the Last Interglacial, The Cryosphere Discussions, 2021, 1–24,
605 https://doi.org/10.5194/tc-2021-6, 2021.

606 Fischer, H., Meissner, K. J., Mix, A. C., Abram, N. J., Austermann, J., Brovkin, V., Capron, E.,
607 Colombaroli, D., Daniau, A.-L., Dyez, K. A., et al.: Palaeoclimate constraints on the impact of 2 C
608 anthropogenic warming and beyond, Nature geoscience, 11, 474, 2018.

609 Govin, A., Capron, E., Tzedakis, P., Verheyden, S., Ghaleb, B., Hillaire-Marcel, C., St-Onge, G.,
610 Stoner, J., Bassinot, F., Bazin, L., Blunier, T., Combourieu-Nebout, N., Ouahabi, A. E., Genty, D.,
611 Gersonde, R., Jimenez-Amat, P., Landais, A., Martrat, B., Masson-Delmotte, V., Parrenin, F.,
612 Seidenkrantz, M.-S., Veres, D., Waelbroeck, C., and Zahn, R.: Sequence of events from the onset to
613 the demise of the Last Interglacial: Evaluating strengths and limitations of chronologies used in
614 climatic archives, Quaternary Science Reviews, 129, 1 – 36,
615 https://doi.org//10.1016/j.quascirev.2015.09.018, 2015.

616 Guarino, M. V., Sime, L., Schroeder, D., Lister, G., and Hatcher, R.: Machine dependence and
617 reproducibility for coupled climate simulations: the HadGEM3-GC3. 1 CMIP Preindustrial
618 simulation, Geoscientific Model Development, 13, 139–154, 2020a.

619 Guarino, M.-V., Sime, L. C., Schröeder, D., Malmierca-Vallet, I., Rosenblum, E., Ringer, M., Ridley,
620 J., Feltham, D., Bitz, C., Steig, E. J., et al.: Sea-ice-free Arctic during the Last Interglacial supports
621 fast future loss, Nature Climate Change, pp. 1–5, 2020b.

622 Hersbach, H, Bell, B, Berrisford, P, et al. The ERA5 global reanalysis. Q J R Meteorol Soc. 2020;
623 146:1999– 2049. https://doi.org/10.1002/qj.3803

624 IPCC: Climate Change 2013: The Physical Science Basis. Contribution of Working Group I to the
625 Fifth Assessment Report of the Intergovernmental Panel on Climate Change. [Stocker, T.F. and Qin,
626 D and Plattner, G and Tignor, M and Allen, S.K. and Boschung, J and Nauels, A and Xia, Y and Bex,
627 V and Midgley, P.M (eds.)], Tech. Rep. 5, Intergovernmental Panel on Climate Change, Cambridge,
628 United Kingdom and New York, NY, USA, https://doi.org/10.1017/CBO9781107415324, 2013.

629 IPCC: Climate Change 2021: The Physical Science Basis. Contribution of Working Group I to the
630 Sixth Assessment Report of the Intergovernmental Panel on Climate Change [Masson-Delmotte, V.,

P. Zhai, A. Pirani, S.L. Connors, C. Pean, S. Berger, N. Caud, Y. Chen, L. Goldfarb, M.I. Gomis, M. Huang, K. Leitzell, E. Lonnoy, J.B.R. Matthews, T.K. Maycock, T. Waterfield, O. Yelekci, R. Yu, and B. Zhou 385 (eds.)], Tech. Rep. 6, Intergovernmental Panel on Climate Change, Cambridge, United Kingdom and New York, NY, USA, 2021.

Kageyama, M., Sime, L. C., Sicard, M., Guarino, M.-V., de Vernal, A., Stein, R., Schroeder, D., Malmierca-Vallet, I., Abe-Ouchi, A., Bitz, C., et al.: A multi-model CMIP6-PMIP4 study of Arctic sea ice at 127 ka: sea ice data compilation and model differences, Climate of the Past, 17, 37–62, 2021.

Kaspar, F., Kühl, N., Cubasch, U., and Litt, T.: A model-data comparison of European temperatures in the Eemian interglacial, Geophysical 390 Research Letters, 32, 2005.

Lunt, D. J., Abe-Ouchi, A., Bakker, P., Berger, A., Braconnot, P., Charbit, S., Fischer, N., Herold, N., Jungclaus, J. H., Khon, V., et al.: A multi-model assessment of last interglacial temperatures, Climate of the Past, 9, 699–717, 2013.

Malmierca-Vallet, I., Sime, L. C., Valdes, P. J., Capron, E., Vinther, B. M., and Holloway, M. D.: Simulating the Last Interglacial Greenland stable water isotope peak: The role of Arctic sea ice changes, Quaternary Science Reviews, 198, 1–14, 395 https://doi.org/doi.org/10.1016/j.quascirev.2018.07.027, 2018.

Meehl, G. A., Senior, C. A., Eyring, V., Flato, G., Lamarque, J.-F., Stouffer, R. J., Taylor, K. E., and Schlund, M.: Context for interpreting equilibrium climate sensitivity and transient climate response from the CMIP6 Earth system models, Science Advances, 6, eaba1981, https://doi.org/10.1126/sciadv.aba1981, 2020.

Notz, D. and the SIMIP Community: Arctic sea ice in CMIP6, Geophysical Research Letters, 47, e2019GL086749, 2020.

Otto-Bliesner, B. L., Rosenbloom, N., Stone, E. J., McKay, N. P., Lunt, D. J., Brady, E. C., and Overpeck, J. T.: How warm was the last interglacial? New model–data comparisons, Philosophical Transactions of the Royal Society A: Mathematical, Physical and Engineering Sciences, 371, 20130097, 2013.

Otto-Bliesner, B. L., Braconnot, P., Harrison, S. P., Lunt, D. J., Abe-Ouchi, A., Albani, S., Bartlein, P. J., Capron, E., Carlson, A. E., Dutton, A., et al.: The PMIP4 contribution to CMIP6–Part 2: Two interglacials, scientific objective and experimental design for Holocene and Last 405 Interglacial simulations, Geoscientific Model Development, 10, 3979–4003, 2017.

Otto-Bliesner, B. L., Brady, E. C., Zhao, A., Brierley, C., Axford, Y., Capron, E., Govin, A., Hoffman, J., Isaacs, E., Kageyama, M., Scussolini, P., Tzedakis, P. C., Williams, C., Wolff, E., Abe-Ouchi, A., Braconnot, P., Ramos Buarque, S., Cao, J., de Vernal, A., Guarino, M. V., Guo, C., LeGrande, A. N., Lohmann, G., Meissner, K., Menviel, L., Nisancioglu, K., O'ishi, R., Salas Y Melia, D., Shi, X., Sicard, M., Sime, L., Tomas, R., Volodin, E., Yeung, N., Zhang, Q., Zhang, Z., and Zheng, W.: Large-scale features of Last Interglacial climate: Results from evaluating the *lig127k* simulations for CMIP6-PMIP4, Climate of the Past Discussions, 2020, 1–41, https://doi.org/10.5194/cp-2019-174, 2020.

Reynolds, R. W., Rayner, N. A., Smith, T. M., Stokes, D. C., and Wang, W.: An improved in situ and satellite SST analysis for climate, J. Climate, 15, 1609–1625, 2002

Sicard, M., A.M. de Boer, and L.C. Sime 2022, Last Interglacial Arctic sea ice as simulated by the latest generation of climate models, Past Global Changes Magazine, 30(2): 92-93

Sime, L., Wolff, E., Oliver, K., and Tindall, J.: Evidence for warmer interglacials in East Antarctic ice cores, Nature, 462, 342–345, 2009.

Turney, C. S. and Jones, R. T.: Does the Agulhas Current amplify global temperatures during super-interglacials?, Journal of Quaternary Science, 25, 839–843, 2010.

Voldoire, A., Saint-Martin, D., Sénési, S., Decharme, B., Alias, A., Chevallier, M., Colin, J., Guérémy, J.-F., Michou, M., Moine, M.-P., et al.: Evaluation of CMIP6 deck experiments with CNRM-CM6-1, Journal of Advances in Modeling Earth Systems, 11, 2177–2213, 2019.